Charge-compensation models of four $Cr^{3+}$ and four $Fe^{3+}$ centres in $KTiOPO_4$



1999 J. Phys.: Condens. Matter 11 3193

(http://iopscience.iop.org/0953-8984/11/15/025)

J. Phys.: Condens. Matter **11** (1999) 3193–3199. Printed in the UK PII: S0953-8984(99)99561-9

# Charge-compensation models of four $Cr^{3+}$ and four $Fe^{3+}$ centres in $KTiOPO_4$

Sang Won Ahn and Sung Ho Choh†

Department of Physics, Korea University, Seoul 136-701, Republic of Korea

Received 23 November 1998

**Abstract.** An overall comparison between the principal-axis orientations of the **g**-tensors and the second-order zero-field-splitting (ZFS) tensors for four $Cr^{3+}$ and four $Fe^{3+}$ centres reported on in our previous studies has been made. One direction of the principal axes of the **g**-tensor is nearly the same as one of those of the second-order ZFS tensor for $Cr^{3+}$ centres, but a similar direction does not exist for $Fe^{3+}$ centres. It is also found that one direction of the principal axes of the second-order ZFS tensors for $Cr^{3+}$ centres is similar to one of those for the $Fe^{3+}$ centres. It is suggested that $Cr^{6+}$ ions substituted for $P^{5+}$ in $PO_4$ tetrahedra play the role of positive monovalent charge compensators for both $Cr^{3+}$ and $Fe^{3+}$, replaced at the sites Ti(1) and Ti(2). Possible charge-compensation models related to $Cr^{6+}$ ions for providing an explanation of the origins of the two different centres arising from the $Cr^{3+}$ and $Fe^{3+}$ at crystallographically equivalent Ti sites are also suggested.

## 1. Introduction

Potassium titanyl phosphate $KTiOPO_4$ (KTP) is a new kind of non-linear optical crystal having a high optical damage threshold [1, 2]. As a result this crystal has been widely applied in areas ranging from frequency doublers [1–4], modulators and Q-switches [5, 6], and low-loss waveguide fabrication [7, 8] to piezoelectric applications [9]. For the last ten years, there have been extensive EPR studies of the crystals carried out in order to provide meaningful information on the microscopic structures around point defects in KTP. KTP crystallizes in the orthorhombic space group $Pna2_1$ with eight formulae per unit cell [10, 11]. The structure exhibits two crystallographically different Ti sites: Ti(1) and Ti(2), replaced by $Cr^{3+}$ and $Fe^{3+}$. Each Ti has four chemically equivalent but magnetically inequivalent sites [12–15] due to the symmetry elements, characterized by two glide planes $\boldsymbol{n}$ and $\boldsymbol{a}$ and one screw axis $2_1$ [10, 11].

On the basis of previous work [16–19], we were able to identify four $Cr^{3+}$ [12, 13] and four $Fe^{3+}$ [14, 15] centres, and all four complete sets of fine structures due to the ions at the magnetically inequivalent sites were systematized in terms of the crystal symmetry of KTP. In this study, an overall comparison between the principal-axis orientations of the **g**-tensors and the second-order zero-field splitting (ZFS) tensors for $Cr^{3+}$ and $Fe^{3+}$ centres is made. Possible charge-compensation models related to $Cr^{6+}$ substituted for $P^{5+}$ in $PO_4$ tetrahedra for providing an explanation of the origins of the two different centres arising from $Cr^{3+}$ and $Fe^{3+}$ at two crystallographically equivalent Ti sites are suggested.

† Author to whom any correspondence should be addressed. E-mail address: `shchoh@kuccnx.korea.ac.kr`; fax: 82-2-927-3292; telephone: 82-2-3290-3091.

0953-8984/99/153193+07$19.50  

## 2. Experiments

For the EPR measurements two kinds of KTP crystal were synthesized by the flux method using the chemical $K_6P_4O_{13}$ [20], known as a particularly suitable flux for growth of KTP crystal [21]. One is nominally undoped and the other is doped with 0.01 mol% of Fe. The $Cr^{3+}$ ions in the undoped crystal were present as an impurity in the starting material and were identified by comparing our EPR results [12, 13] with those given in reference [18].

The EPR measurements were carried out at room temperature by employing a Bruker Q-band spectrometer [12, 14]. It is critical to establish an accurate crystal orientation with respect to the applied magnetic field in order to properly classify several centres having similar EPR parameters and all four fine structures belonging to each centre. Two sets of fine-structure lines became degenerate forming one set when the magnetic field $\boldsymbol{B}$ was applied in each of the crystallographic planes $ab$, $bc$, and $ca$. All four sets due to each of $Cr^{3+}$ and $Fe^{3+}$ at the four magnetically inequivalent sites merged completely into one when $\boldsymbol{B}$ was aligned along each of the crystal axes $\boldsymbol{a}$, $\boldsymbol{b}$, and $\boldsymbol{c}$. This made it possible to establish crystal alignments within $\pm 0.05^\circ$ in the three planes by adjusting the crystal orientation inside the cylindrical cavity in such a way as to achieve degeneracy of the EPR lines [12, 14]. The EPR spectra were recorded by varying the orientations of $\boldsymbol{B}$ in the three planes from $0^\circ$ to $180^\circ$ in steps of $3^\circ$ for the $Fe^{3+}$ spectra and $4^\circ$ for the $Cr^{3+}$ spectra.

## 3. Results and discussion

Depending on the value of the effective spin $S$ of a paramagnetic ion and the symmetry around the substitutional ion, different numbers of the spin-Hamiltonian terms are required for a satisfactory description of the EPR spectra and their angular dependences [22]. For an $Fe^{3+}$ ion with the effective spin $S = 5/2$ at a triclinic site in KTP, the appropriate spin Hamiltonian is given by [14, 15, 18]

$$H_S = \sum_{ij} \mu_B B_i g_{ij} S_j + \sum_{m=-2}^{2} B_2^m O_2^m + \sum_{m=-4}^{4} B_4^m O_4^m \tag{1}$$

where the first term represents the electron Zeeman interaction and the others the ZFS or the fine structure. Six independent elements for the **g**-tensor, five for the second-order ZFS tensor, and nine for the fourth-order ZFS tensor are needed to describe the $Fe^{3+}$ spectra. On the order hand, for $Cr^{3+}$ with $S = 3/2$ only the first two terms of equation (1) are needed [18, 19]. For all $Cr^{3+}$ and $Fe^{3+}$ spectra, the necessary spin-Hamiltonian parameters were determined [12–15] by employing a computer program, EPR-NMR [23]. The detailed procedure for calculating these parameters was described in [12, 14]. For each of the $Cr^{3+}$ and $Fe^{3+}$ centres, sixteen sets of fine structures were identified, and the sets were divided into four groups having the same principal values but different principal-axis orientations of **g** and the second-order ZFS tensors [12–15]. The groups were denoted as the centres A, B, C, and D for $Cr^{3+}$ [12, 13], and C1, C2, C3, and C4 for $Fe^{3+}$ [14, 15], each of which contains four fine structures arising from each of $Cr^{3+}$ and $Fe^{3+}$ at magnetically inequivalent sites.

For each of the fine structures, the program yields two sets of principal-axis orientations of each of the **g**-tensors and the second-order ZFS tensors represented in right-handed or left-handed coordinates, where each combination of them can be chosen as a set of principal axes. For comparison between the EPR data for $Cr^{3+}$ and $Fe^{3+}$, all sets are now chosen to be represented in right-handed coordinates: the orientations of the **g**-tensors for SA1 and SB1 [12] and the second-order ZFS tensors for SA1 and SC1 [13] represented in left-handed coordinates are now converted into ones in right-handed-coordinate representations. The theta

**Table 1.** Principal-axis orientations of $\boldsymbol{g}$-tensors and the second-order ZFS tensors with respect to the crystallographic axes ($\boldsymbol{a}$, $\boldsymbol{b}$, $\boldsymbol{c}$) for $Cr^{3+}$ in $KTiOPO_4$, and pairs of the principal axes having similar orientations of the two tensors for each centre and the angles between them.

| | $A_I^{Cr}$(SB1) | | $B_I^{Cr}$(SD1) | | $C_I^{Cr}$(SA1) | | $D_I^{Cr}$(SC1) | |
|---|---|---|---|---|---|---|---|---|
| | Orientations (deg) of the principal axes of $\boldsymbol{g}$-tensors[a] | | | | | | | |
| | $\theta$ | $\phi$ | $\theta$ | $\phi$ | $\theta$ | $\phi$ | $\theta$ | $\phi$ |
| O$x'$ | 131 | 349 | 142 | 350 | 103 | 86 | 63 | 217 |
| O$y'$ | 139 | 183 | 119 | 214 | 14 | 107 | 139 | 271 |
| O$z'$ | 97 | 85 | 112 | 111 | 85 | 357 | 62 | 323 |
| | Orientations (deg) of the principal axes of the second-order ZFS tensors[b] | | | | | | | |
| | $\theta$ | $\phi$ | $\theta$ | $\phi$ | $\theta$ | $\phi$ | $\theta$ | $\phi$ |
| O$x$ | 53.88 | 350.70 | 51.47 | 354.95 | 67.48 | 261.63 | 50.96 | 268.35 |
| O$y$ | 143.72 | 345.64 | 41.17 | 346.53 | 157.45 | 265.07 | 140.94 | 270.66 |
| O$z$ | 92.89 | 79.57 | 94.12 | 81.66 | 88.78 | 352.14 | 88.87 | 359.27 |
| | Pairs and angles (deg)[a] | | | | | | | |
| | (O$z'$, O$z$); 7 | | (O$x'$, O$y$); 3 | | (O$z'$, O$z$); 6 | | (O$y'$, O$y$); 2 | |

[a] The estimated maximum uncertainties in the angle are $\pm 2.6^\circ$ for all centres.
[b] The estimated maximum uncertainties in the angle are $\pm 0.05^\circ$ for all centres.

values of the principal axes of the **g**-tensor are $\boldsymbol{x}'$ for SC1 and $\boldsymbol{z}'$ for SD1 (with the typographical errors in [13] corrected). After comparison of the principal-axis orientations among 16 fine structures, a representative fine structure having the closest principal-axis orientations to the other three representative ones have been chosen for each centre. After overall conversion, the principal-axis orientations of the **g**-tensors and the second-order ZFS tensors with respect to the crystallographic axes for the $Cr^{3+}$ centres are listed in table 1, where the centres B, D, A, and C from our previous reports [12, 13] are renamed as $A^{Cr}$, $B^{Cr}$, $C^{Cr}$, and $D^{Cr}$, respectively. The subscripts, i = I, II, III, and IV, indicate the fine structures due to the $Cr^{3+}$ substituted at four magnetically inequivalent Ti sites, I, II, III, and IV, respectively [12–15]. The line intensities of $A^{Cr}$ and $C^{Cr}$ are much stronger than those of $B^{Cr}$ and $D^{Cr}$ [13].

The orientations of the principal axes $\boldsymbol{x}$, $\boldsymbol{y}$, and $\boldsymbol{z}$ of the second-order ZFS tensors for $A^{Cr}$ and $B^{Cr}$ nearly coincide with those of the Ti(1)–O(2), Ti(1)–O(1), and Ti(1)–O(6) bonds, respectively, and those for $C^{Cr}$ and $D^{Cr}$ nearly coincide with those of the bonds Ti(2)–OT(1) (rather than Ti(2)–OT(2) as given in [13]), Ti(2)–O(8), and Ti(2)–O(4), respectively. From this result it was concluded that the centres $A^{Cr}$ and $B^{Cr}$ as well as $C^{Cr}$ and $D^{Cr}$ with similar principal-axis orientations originate from $Cr^{3+}$ at the sites Ti(1) and Ti(2), respectively [13]. For each centre, one principal-axis direction of the **g**-tensors is nearly the same as one of those of the second-order ZFS tensor. For the two quantities, the pairs of similar principal axes of **g** and the second-order ZFS tensors are as follows: $\boldsymbol{z}'$ and $\boldsymbol{z}$ for $A_I^{Cr}$ and $C_I^{Cr}$, $\boldsymbol{x}'$ and $\boldsymbol{y}$ for $B_I^{Cr}$, and $\boldsymbol{y}'$ and $\boldsymbol{y}$ for $D_I^{Cr}$ as listed in table 1.

The principal-axis orientations of $Fe^{3+}$ centres have been chosen like those of $Cr^{3+}$: the orientations of the second-order ZFS tensors of C1 and C3, named in [14, 15], have now been chosen from another set of two yielded by the computer program [23]. The principal-axis orientations of the second-order ZFS tensors with respect to the crystallographic axes for the $Cr^{3+}$ and the $Fe^{3+}$ centres are listed in table 2, where the centres called C1, C3, C2, and C4 in [14, 15] are renamed as $A^{Fe}$, $B^{Fe}$, $C^{Fe}$, and $D^{Fe}$, respectively. The line intensities of $A^{Fe}$ and $C^{Fe}$ are much stronger than those of $B^{Fe}$ and $D^{Fe}$, like those of the $Cr^{3+}$ centres. The

**Table 2.** Principal values of the second-order ZFS tensors and their principal-axis orientations with respect to the crystallographic axes ($\boldsymbol{a}$, $\boldsymbol{b}$, $\boldsymbol{c}$) for $Cr^{3+}$ and $Fe^{3+}$ in $KTiOPO_4$, and pairs of the principal axes having similar orientations of $Cr^{3+}$ and $Fe^{3+}$ centres and the angles between them.

| | $Cr^{3+}$ centres | | | | | | | |
|---|---|---|---|---|---|---|---|---|
| | $A_I^{Cr}$(SB1) | | $B_I^{Cr}$(SD1) | | $C_I^{Cr}$(SA1) | | $D_I^{Cr}$(SC1) | |
| | Principal values of the second-order ZFS tensors[a] | | | | | | | |
| $B_2^0$ ($cm^{-4}$) | 1365.4 | | 1259.4 | | 1675.7 | | 1451.4 | |
| $B_2^2$ ($cm^{-4}$) | 1194.9 | | 1227.7 | | 932.4 | | 1361.1 | |
| $N_2$ ($cm^{-8}$) | 2340246 | | 2088504 | | 3097760 | | 2724093 | |
| | Orientations (deg) of the principal axes of the second-order ZFS tensors[b] | | | | | | | |
| | $\theta$ | $\phi$ | $\theta$ | $\phi$ | $\theta$ | $\phi$ | $\theta$ | $\phi$ |
| O$x$ | 53.88 | 350.70 | 51.47 | 354.95 | 67.48 | 261.63 | 50.96 | 268.35 |
| O$y$ | 143.72 | 345.64 | 141.17 | 346.53 | 157.45 | 265.07 | 140.94 | 270.66 |
| O$z$ | 92.89 | 79.57 | 94.12 | 81.66 | 88.78 | 352.14 | 88.87 | 359.27 |
| | $Fe^{3+}$ centres | | | | | | | |
| | $A_I^{Fe}$(C1b) | | $B_I^{Fe}$(C3b) | | $C_I^{Fe}$(C2a) | | $D_I^{Fe}$(C4a) | |
| | Principal values of the second-order ZFS tensors[a] | | | | | | | |
| $B_2^0$ ($cm^{-4}$) | −817.3 | | −819.3 | | −739.1 | | −722.5 | |
| $B_2^2$ ($cm^{-4}$) | −443.1 | | −439.8 | | −442.2 | | −552.9 | |
| $N_2$ ($cm^{-8}$) | 733425 | | 735727 | | 611449 | | 623906 | |
| | Orientations (deg) of the principal axes of the second-order ZFS tensors[b] | | | | | | | |
| | $\theta$ | $\phi$ | $\theta$ | $\phi$ | $\theta$ | $\phi$ | $\theta$ | $\phi$ |
| O$x$ | 66.23 | 260.98 | 65.88 | 260.70 | 67.84 | 258.15 | 63.26 | 259.43 |
| O$y$ | 132.45 | 327.22 | 132.68 | 326.54 | 140.02 | 319.09 | 138.00 | 315.41 |
| O$z$ | 51.83 | 11.23 | 51.91 | 17.17 | 58.65 | 2.51 | 60.31 | 6.13 |
| | Pairs and angles (deg)[b] | | | | | | | |
| | $A_I^{Cr}$ (O$x$), $C_I^{Fe}$ (O$z$); 10.9 | | $B_I^{Cr}$ (O$x$), $C_I^{Fe}$ (O$z$); 9.4 | | $C_I^{Cr}$ (O$x$), $A_I^{Fe}$ (O$x$); 1.4 | | $D_I^{Cr}$ (O$x$), $A_I^{Fe}$ (O$x$); 16.5 | |
| | $A_I^{Cr}$ (O$x$), $D_I^{Fe}$ (O$z$); 14.4 | | $B_I^{Cr}$ (O$x$), $D_I^{Fe}$ (O$z$); 12.3 | | $C_I^{Cr}$ (O$x$), $B_I^{Fe}$ (O$x$); 1.8 | | $D_I^{Cr}$ (O$x$), $B_I^{Fe}$ (O$x$); 16.5 | |
| | — | | — | | $C_I^{Cr}$ (O$x$), $C_I^{Fe}$ (O$x$); 3.3 | | — | |
| | — | | — | | $C_I^{Cr}$ (O$x$), $D_I^{Fe}$ (O$x$); 4.7 | | — | |

[a] The estimated maximum uncertainties in the angle are $\pm 0.3^\circ$ for all centres.
[a] The estimated maximum uncertainties in the angle are $\pm 0.05^\circ$ for all centres and all pairs.

representative fine structures $A_I^{Fe}$ and $B_I^{Fe}$ correspond to C1b and C3b. For a paramagnetic ion with $S \geqslant 5/2$ at a triclinic site, the symmetry of the fourth-order ZFS terms mainly reflects that of the nearest neighbours around the substitutional-ion sites [24, 25]. Therefore, in this case, unlike that of $Cr^{3+}$, a comparison of the orientations of the principal axes between the second-order ZFS tensors and the Ti–O bonds cannot provide an indicator for identifying the origin of the centres. By comparing the result [18] obtained from pseudosymmetry-axis method [24, 25] and our previous results [14, 15], the centres $A^{Fe}$ and $B^{Fe}$ were found to arise from $Fe^{3+}$ at Ti(1), and $C^{Fe}$ and $D^{Fe}$ from $Fe^{3+}$ at Ti(2). Unlike the case for $Cr^{3+}$, the **g**-tensor and the second-order ZFS tensor of the $Fe^{3+}$ centre do not have any similar principal-axis directions. For each centre, however, one principal-axis direction of the second-order ZFS tensor of $Cr^{3+}$ is nearly the same as one of those of $Fe^{3+}$. For the two quantities, the pairs of similar axes are listed in table 2.

Since the norm defined in [22] is invariant under arbitrary rotations of the frame of coordinates, it is useful to examine the equivalency of the centres represented in various coordinate systems. In addition to the norm, an investigation of the closeness of the mutual orientations of two vectors measured in terms of the normalized scalar product of the principal-axis orientations of the second-order ZFS tensors is also useful, for examining the equivalency [26]. From the closeness of the numerically defined norm and the mutual orientation, it was concluded in [26] that the two centres $A^M$ and $B^M$ are equivalent. However, in the case of the four $Cr^{3+}$ and the four $Fe^{3+}$ centres in KTP with very similar orientations of the second-order ZFS tensors, the two numerical definitions are not sufficient to allow us to reach such a conclusion. One of the most reliable pieces of evidence for the non-equivalency of the four centres can be obtained by a consideration of the following two facts: (i) $A^M$ and $C^M$ have conspicuously stronger line intensities than $B^M$ and $D^M$ [12–15], and (ii) the four complete sets of fine-structure lines arising from $Cr^{3+}$ and $Fe^{3+}$ are observed at magnetically inequivalent sites in the skew planes which deviate slightly from the three crystallographic planes. On the basis of this evidence we have reached the conclusion that the four $Cr^{3+}$ and the four $Fe^{3+}$ centres are definitely distinct.

As an explanation as to why such kinds of the two different centres arise from the crystallographically equivalent Ti sites, a vacancy of the first-neighbour oxygen OT(1) was suggested as a divalent positive charge compensator simultaneously for the two $Cr^{3+}$ ions and the two $Fe^{3+}$ ions at the adjacent Ti(1) and Ti(2) sites [13, 15]. In this case, the closeness of the second-order ZFS tensor data sets for the two $Cr^{3+}$ centres and two $Fe^{3+}$ centres would be hard to understand, since the vacancy would force the original Ti–O orientations to be substantially deformed. As a result, the two centres would have quite different orientations of the principal axes of the second-order ZFS tensors and their principal values. Consequently, this type of charge compensator is more likely to be placed beyond the first neighbour around the substitutional $Cr^{3+}$ and $Fe^{3+}$ ions.

The electron-trapping $Cr^{5+}$ centres and hole centres $[HCrO_3]^-$ were observed at about 173 K in chromium-doped KTP after it had been irradiated with x-rays at room temperature [27], and $Cr^{6+}$ was found to be substituted for $P^{5+}$ in a slightly distorted tetrahedron, $P^{5+}(O^{2-})_4$. In addition to this result, a more probable origin of the four centres than previous ones [13, 15] is illustrated in figure 1. The ionic radius of $Ti^{4+}$ (0.68 Å) is very similar to that of $Cr^{3+}$ (0.63 Å), but the charge states of the two ions are different. When $Cr^{3+}$ ions substitute for Ti sites, these defect centres should be compensated by a monovalent charge for each of the $Cr^{3+}$ ions to achieve electrical neutrality. A $Cr^{6+}$ ion substituted for $P^{5+}$ may be a good monovalent charge compensator. The original P–O bond orientations in the $PO_4$ octahedron may be somewhat deformed by the substitutional $Cr^{6+}$ ion, with its ionic radius (0.52 Å) being larger than that of $P^{5+}$ (0.35 Å); however, the original Ti–O structures may not be disturbed

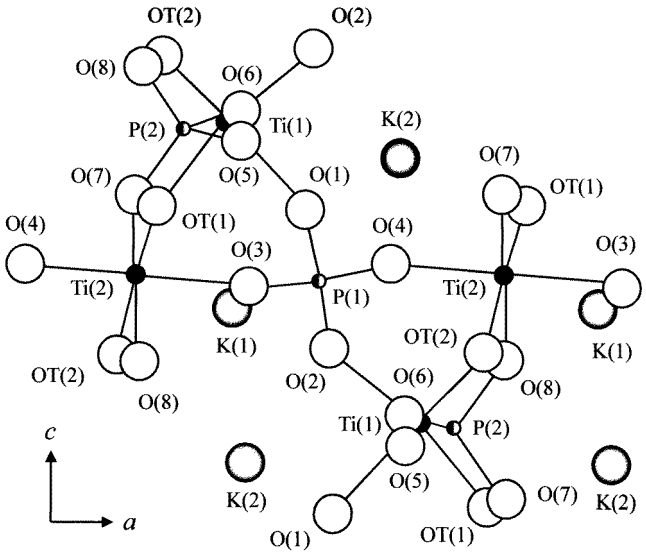


a) $A^M$: $Ti^{4+}(1)-O(1)-P^{5+}(1) \longrightarrow M^{3+}-O(1)-Cr^{6+}$ or
$Ti^{4+}(1)-O(6)-P^{5+}(2) \longrightarrow M^{3+}-O(6)-Cr^{6+}$

b) $C^M$: $Ti^{4+}(2)-O(3)-P^{5+}(1) \longrightarrow M^{3+}-O(3)-Cr^{6+}$ or
$Ti^{4+}(2)-O(7)-P^{5+}(2) \longrightarrow M^{3+}-O(7)-Cr^{6+}$

c) $B^M$ & $D^M$: $Ti^{4+}(1)-O(1)-P^{5+}(2)$ & $Ti^{4+}(2)-O(3)-P^{5+}(1)$
$\longrightarrow M^{3+}-O(1)-Cr^{6+}$ & $M^{3+}-O(3)-Cr^{6+}$

**Figure 1.** Projection of the KTP structure on the *ca*-plane, and the charge-compensation models. The substitutional $M^{3+}$ (M = Cr or Fe) sites and $Cr^{6+}$ sites playing the role of charge compensators are as follows: (a) $M^{3+}$ at Ti(1), $Ti^{4+}$ at Ti(2), and $Cr^{6+}$ at P(1) or P(2) for $A^M$; (b) $Ti^{4+}$ at Ti(1), $M^{3+}$ at Ti(2), and $Cr^{6+}$ at P(1) or P(2) for $C^M$; and (c) $M^{3+}$ simultaneously at Ti(1) and Ti(2) as well as $Cr^{6+}$ simultaneously at P(1) and P(2) for both centres $B^M$ and $D^M$.

very much by this charge compensator. Such $Cr^{6+}$ ions can play the role of monovalent charge compensators with little deformation of the Ti–O bond orientations as shown in figure 1. The probability of $Cr^{3+}$ ions being substituted simultaneously at both Ti sites (case (c)) might be much less than that of them being substituted at either Ti(1) or Ti(2) sites. The centres $A^M$ and $C^M$ with comparatively much stronger intensities appear to be originating from the more abundant $Cr^{3+}$ ions in cases (a) and (b). Nevertheless, there are two possibilities for assigning a certain site of the charge compensator $Cr^{6+}$ to $A^M$ and $C^M$ using the present data alone. This charge-compensation model shown in figure 1 can be applied to $Fe^{3+}$ (0.64 Å) centres on the basis of the fact that $Cr^{3+}$ spectra are also present for the Fe-doped KTP crystal.

In summary, it has been found that the two numerically defined norms [22] and the normalized scalar product of the principal-axis orientations of the second-order ZFS tensors [26] are not very useful for investigating the equivalency of the four distinct $Cr^{3+}$ centres and the four $Fe^{3+}$ centres in KTP. It has been found that one principal-axis direction of the **g**-tensor is nearly the same as one of those of the second-order ZFS tensor for $Cr^{3+}$ centres, and one

principal-axis direction of the second-order ZFS tensor for $Cr^{3+}$ centres is also similar to one of those for the $Fe^{3+}$ centres. A $Cr^{6+}$ ion substituted for $P^{5+}$ in a $PO_4$ tetrahedron plays the role of a positive monovalent charge compensator to achieve electrical neutrality when $Cr^{3+}$ and $Fe^{3+}$ ions substitute at Ti(1) or Ti(2) sites. The similar orientations of the principal axes of the second-order ZFS tensors of $A^M$ and $B^M$ as well as $C^M$ and $D^M$, arising from M (M = Cr or Fe) at the respective Ti(1) and Ti(2) sites, are well explained by the suggested charge-compensation models in connection with the $Cr^{6+}$ ions substituting for $P^{5+}$ ions.

## Acknowledgments

This work was partially supported by the Korea Science and Engineering Foundation through the Research Centre for Dielectric and Advanced Matter Physics at Pusan National University (1997-2000). S W Ahn is grateful to Korea University for a Postdoctoral Fellowship (1998–1999).

## References

[1] Zumsteg F C, Bierlein J D and Gier T E 1976 *J. Appl. Phys.* **47** 4980
[2] Bierlein J D and Vanherzeele H 1989 *J. Opt. Soc. Am.* B **6** 622
[3] Risk W P, Payne R N, Lenth W, Harder C and Meier H 1989 *Appl. Phys. Lett.* **55** 1179
[4] Wang X D, Basseras P, Miller R J D and Vanherzeele H 1991 *Appl. Phys. Lett.* **59** 519
[5] Massey G A, Loehr T M, Willis L J and Johnson J C 1980 *Appl. Opt.* **19** 4136
[6] Bierlein J D and Arweiler C B 1986 *Appl. Phys. Lett.* **49** 917
[7] Laurell F, Roelofs M G, Bindloss W, Hsiung H, Suna A and Bierlein J D 1992 *J. Appl. Phys.* **71** 4664
[8] Eger D, Oron M and Katz M 1993 *J. Appl. Phys.* **74** 4298.
[9] Chu D K T, Bierlein J D and Hunsperger R G 1992 *IEEE Trans. Ultrason. Ferroelectr. Freq. Control* **39** 683
[10] Tordjman I, Masse R and Guitel J C 1974 *Z. Kristallogr.* **139** 103
[11] Thomas P A, Glazer A M and Watts B E 1990 *Acta Crystallogr.* B **46** 333
[12] Ahn S W, Choh S H and Kim J N 1995 *J. Phys.: Condens. Matter* **7** 667
[13] Ahn S W, Choh S H and Rudowicz C 1997 *Appl. Magn. Reson.* **12** 351
[14] Ahn S W, Choh S H and Choi B C 1995 *J. Phys.: Condens. Matter* **7** 9615
[15] Ahn S W and Choh S H 1998 *J. Phys.: Condens Matter* **10** 341
[16] Khasanova N M, Nizamutdinov N M, Izugzon A S, Bulka G R, Vinokurov V M, Pavlova N I and Rez I S 1988 *Physics of Minerals and Synthetic Crystals* (Kazan: Kazan University Press) p 87 (in Russian)
[17] Galeev A A, Nizamutdinov N M, Bulka G R, Khasanova N M, Pavlova N I, Ermakov G A and Vinokurov V M 1990 *Spectroscopy, Crystal Chemistry and Real Structure of Minerals and their Analogues* (Kazan: Kazan University Press) p 140 (in Russian)
[18] Gaite J M, Stenger J F, Dusausoy Y, Marnier G and Rager H 1991 *J. Phys.: Condens. Matter* **3** 7877
[19] Stenger J F, Dusausoy Y, Marnier G, Rager H and Gaite J M 1989 *J. Phys.: Condens. Matter* **1** 4643
[20] Choi B C, Kim J B, Yun S I and Kim J N 1993 *Korean Appl. Phys.* **6** 27
[21] Bolt R J, De Hass H, Sebastian M T and Klapper H 1991 *J. Cryst. Growth* **110** 587
[22] Rudowicz C 1987 *Magn. Reson. Rev.* **13** 1
[23] Mombourquette M J, Weil J A and McGavin D G 1994 *Operating Instructions for Computer Program EPR-NMR (Version 6.0)* Department of Chemistry, University of Saskatchewan, Canada
[24] Michoulier J and Gaite J M 1972 *J. Chem. Phys.* **56** 5205
[25] Gaite J M and Michoulier J 1973 *J. Chem. Phys.* **59** 488
[26] Rudowicz C, Akhmadoullin I and Madhu S B 1997 *Proc. 1st Asia–Pacific EPR/ESR Symp. (Hong Kong)* (Hong Kong: Springer) p 578
[27] Markelov A A, Nizamutdinov N M, Hasanova N M, Pavlova N I, Vanishtein D I, Vinokurov V M, Garmash V M 1988 *Physics of Minerals and Synthetic Crystals* (Kazan: Kazan University Press) p 63 (in Russian)